NASA TECHNICAL MEMORANDUM NASA TM-76710

INFLUENCE OF THE REYNOLDS NUMBER ON THE NORMAL FORCES OF SLENDER BODIES OF REVOLUTION

Klaus Hartmann

Translation of "Ueber den Einfluss der Reynoldszahl auf die Normalkraefte schlanker Flugkoerperruempfe". Zeitschrift fur Flugwissenschaften und Weltraumforschung., Vol. 2, No. 1, 1978, pp 22-35.

NATIONAL AERONAUTICS AND SPACE ADMINISTRATION
WASHINGTON D.C. 20546 MAY 1982

STANDARD TITLE PAGE

1. Report No.	2. Government Accession No.	3. Recipient's Catalog No.
NASA TM-76710		

4. Title and Subtitle	5. Report Date
INFLUENCE OF THE REYNOLDS NUMBER ON NORMAL FORCES OF SLENDER BODIES OF REVOLUTION	MAY 1982
	6. Performing Organization Code
7. Author(s)	8. Performing Organization Report No.
Klaus Hartmann	10. Work Unit No.
	11. Contract or Grant No. NASw- 3542
9. Performing Organization Name and Address SCITRAN Box 5456 Santa Barbara, CA 93108	13. Type of Report and Period Covered Translation
12. Sponsoring Agency Name and Address National Aeronautics and Space Administration Washington, D.C. 20546	14. Sponsoring Agency Code

15. Supplementary Notes

Translation of "Ueber den Einfluss der Reynoldszahl auf die Normalkraefte schlanker Flugkoerperruempfe". Zeitschrift fur Flugwissenschaften und Weltraumforschung, Vol. 2, No. 1, 1978, pp 22-35.

16. Abstract

Flow over slender bodies of revolution is strongly influenced by three-dimensional vortex separation. The influence of the Reynolds number on nonlinear normal forces of slender bodies of revolution is investigated. Experiments were carried out at the Transonic Wind Tunnel and the High Speed Wind Tunnel of the DFVLR/AVA. Experimental results are analyzed theoretically.

17. Key Words (Selected by Author(s))	18. Distribution Statement
	Unclassified - Unlimited

19. Security Classif. (of this report)	20. Security Classif. (of this page)	21. No. of Pages	22. Price
Unclassified	Unclassified	29	

INFLUENCE OF THE REYNOLDS NUMBER ON THE NORMAL FORCES OF SLENDER BODIES OF REVOLUTION

Klaus Hartmann* DFVLR/AVA Goettingen**

***/22

Übersicht: Die Strömung um schlanke Flugkörperrümpfe bei großen Anstellwinkeln wird stark beeinflußt durch dreidimensio nale Wirbelablösungen. Infolgedessen hängen die aerodynamischen Kräfte nichtlinear vom Anstellwinkel ab. Von entscheiden dem Einfluß auf die aerodynamischen Kräfte ist der Zustand der Grenzschicht an den Ablösestellen (laminar oder turbulent). Da durch ist eine erhebliche Abhängigkeit der Strömung von der Reynoldszahl bedingt. Die Lage der Ablöselinien ergibt sich aus de Wechselwirkung zwischen der Grenzschicht und der äußeren abgelösten Strömung. Das führt dazu, daß die Berechnung de aerodynamischen Kräfte von Flugkörperrümpfen bei großen Anstellwinkeln auf rein theoretischem Wege zur Zeit nicht mög lich ist. Deshalb ist es auch heute noch notwendig, durch gezielte systematische Windkanaluntersuchungen die bisherigen Kennt nisse über die komplizierte Rumpfumströmung zu erweitern und zu vertiefen. Ausgehend davon sind bestehende Berechnungs verfahren verbessert und neue Verfahren ausgearbeitet worden. Zur Untersuchung des Einflusses der Reynoldszahl auf di Normalkräfte wurden an Flugkörperrümpfen bei Anstellwinkeln bis zu 90° im Machzahlbereich Ma_∞ = 0,5 bis 2,2 bei variable Reynoldszahl im Transsonischen Windkanal und im Hochgeschwindigkeitswindkanal der DFVLR/AVA umfangreiche Kraft und Momentenmessungen, Druckverteilungsmessungen sowie Experimente zur Strömungssichtbarmachung durchgeführt. Di experimentellen Ergebnisse wurden einer theoretischen Analyse unterzogen. Dabei konnte eine halbempirische Theorie ent wickelt werden, welche die Versuchsergebnisse befriedigend beschreibt.

Influence of the Reynolds number on the normal forces of slender bodies of revolution

Summary: The flow over slender bodies of revolution at high angles of attack is strongly influenced by three-dimensional vorte separation. As a result of separation the aerodynamic forces increase in a nonlinear way with the angle of attack. The state of th boundary layer at the separation lines has a striking influence on the aerodynamic forces which therefore depend considerably on the Reynolds number. The position of the separation lines is not known a priori but evolves from the interaction between th boundary layer and the outer separated flow. Due to the complexity of this flow, the theoretical calculation of aerodynamic forces for bodies of revolution at high angles of attack is not yet possible. It is therefore still necessary to extend the present knowledge about the complicated flow over bodies of revolution by systematic wind-tunnel investigations. On the basis of these investigations existing computational methods have been improved and new methods have been worked out. In this paper the influence of the Reynolds number on nonlinear normal forces of slender bodies of revolution is investigated. For this purpose comprehensive force-, moment- and pressure-distribution measurements as well as flow visualization experiments were carried out in the Transonic Wind Tunnel and in the High-Speed Wind Tunnel of the DFVLR/AVA for bodies of revolution at angles of attack up to 90° in the Mach number range Ma_∞ = 0.5 to 2.2 at variable Reynolds number. The experimental results were analysed theoretically and an empirical theory could be developed which describes the test results satisfactorily.

---

*) Shortened version of the dissertation of the author [1] approved by the faculty for Mechanical Engineering and Electrical Technology of the University of Braunschweig (referant H. Schlichting and Prof. H. Ludwieg).

**) Dr. Klaus Hartmann, Institute for Fluid Mechanics of the German Research and Test Facility for Aerodynamics and Space Flight DFVLR/AVA, Bunsenstr. 10, 3400 Goettingen.

***) Numbers in margin indicate pagination of foreign text.

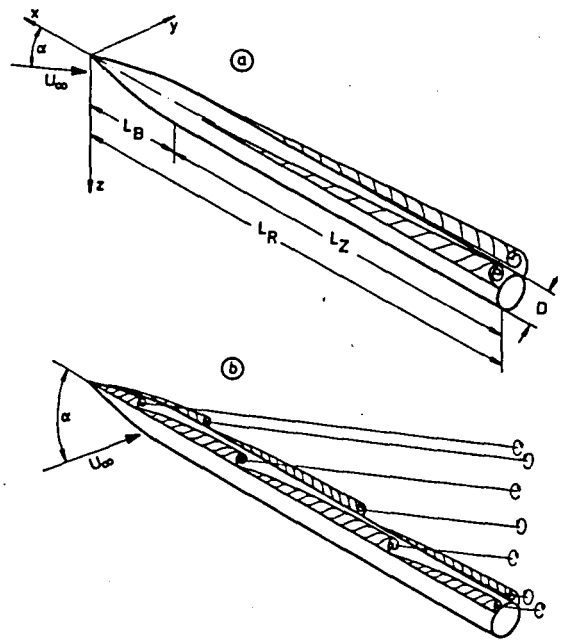

Figure 1. Schematic representation of vortex formation for flow around slender bodies.
a) symmetric vortex separation for small angles of attack
b) asymmetric vortex separation for large angles of attack

Pressure measurements and experiments for flow visualization of body models were performed. An attempt was made to analyze the experimental results using a semi-empirical theory*.

2. Notation

2.1 Geometric variables (see Figures 1-4).

D	body diameter = reference length (= 2R)
L_B	nose length (Ogive) =(3D or 1.5 D)
L_R	total body length (= 19 D and 21.5 D)
L_Z	body length without Ogive
$r_w(x)$	distance of the body vortex centers from the body longitudinal axis (see Figure 4)

*The suggestion for this work evolved from a collaboration with the Royal Aircraft Establishment, Farnborough, England, over many years and the German aviation industry, especially the firm Messerschmitt-Boelkow-Blohm, Ottobrunn near Munich.

S	base area of body = reference area $(= \pi D^2/4)$
x, y, z	rectangular coordinate system of a body--fixed axis system with origin at the body tip (see Figure 1)
x_B	nose length $(= L_B)$
Φ	polar angle (see Figure 3)
$\Phi_{1.Abl.}$	polar angle of primary separation (see Figure 3)
$\Phi_{2.Abl.}$	polar angle of secondary separation (see Figure 3)

2.2 Aerodynamic variables

C_p	coefficient of static pressure along the body surface $[= (p - p_\infty)/q_\infty]$
C_W	drag coefficient of an infinitely long circular cylinder in a transverse flow $(= W'/q_\infty D)$
$(C_W)_{nl.}$	drag coefficient of the nonlinear normal force part
$c_Z(x/D)$	local normal force coefficient
$-C_Z$	normal force coefficient $(= C_N = N/q_\infty S)$
$(C_Z)_{nl.}$	nonlinear normal force coefficient
N	normal force
W'	drag per length unit of an infinitely long circular cylinder in transverse flow
α	angle of attack (see Figure 1)
$\alpha_{Str.}, (\alpha_{Str.})_{th}$	experimental and theoretical streamline angle

2.3 Flow variables

Ma_∞	Mach number of flow
Ma_Q	Mach number of transverse flow $(= Ma_\infty \sin\alpha)$
$Ma_{Q,krit.}$	critical transverse flow Mach number
p	static pressure on body surface
p_∞	static pressure of incident flow
q_∞	stagnation pressure of incident flow $[= (\varrho/2) U_\infty^2]$
Re_D	Reynolds number referred to D $(= U_\infty D/\nu_\infty)$
Re_{eff}	effective Reynolds number $(= Re_D/\sin\alpha)$
U_∞	incident flow speed
U_Q	transverse flow speed $(= U_\infty \sin\alpha)$
ν_∞	kinematic viscosity of incident flow
ϱ_∞	density of incident air

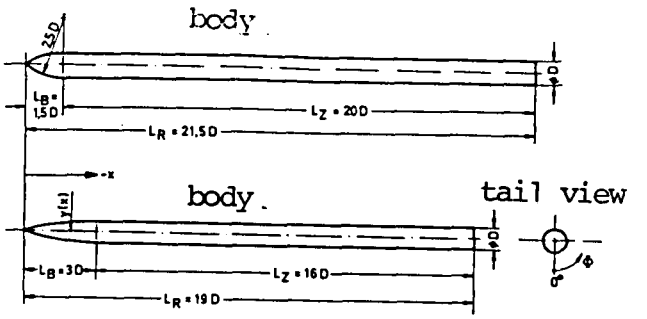

contour of ogive according to

Figure 2. Geometric data for models, body 1 and body 2

TABLE 1. Range of experimental investigations

Model	type of investigation	Ma_∞	$10^{-5}\,Re_D$	α [°]
body 2 3 *D*-Ogive	force and moment measurements	0.5, 0.7, 0.8	1.1; 1.3; 1.4; 2: 3; 4; 5.4; 6.4; 7.9; 8.4	$0 \leqq \alpha \leqq 90$
		1	3 1.9; 2.2; 3.9; 5.3; 6.4	$0 \leqq \alpha \leqq 30$ 10, 20, 30
		1.79	2.9 2.2; 3.7; 4.3	$0 \leqq \alpha \leqq 30$ 10, 20, 30
body 1 1.5 *D*-Ogive	pressure distribution measurements	0.7	5.2	5, 10, 15, 20, 25, 30
		0.8	5.6	20
		1	6.1	10, 20, 30
body 2 3 *D*-Ogive	pressure distribution measurements	1, 1.46, 1.79, 2.21	3	5, 10, 15, 20, 25, 30
		1	1.6; 2.2; 3; 3.9; 5.3; 6.4; 7	10, 20, 30
		1.79	2.2; 3.0; 3.7; 4.6	10, 20, 30
	smoke photographs	0.6	5.5	20
	paint images	0.8	5.5	5, 10, 15
body 1 1.5 *D*-Ogive	paint images	0.7	5.7	20, 25, 30, 45

3. Results of experimental investigations

3.1 Models, test facilities and range of investigations

The experimental results were obtained from two different models called body 1 and body 2 over several test programs extending over some time [2,3,4]. Both body models differ in terms of the degree of slenderness L_B/D (= 1,5 and 3) and the contour of their nose shapes (ogives). They also differ slightly in terms of total length L_R (= 19 D and 21.5 D). The geometric details of both bodies are shown in Figure 2. The models were made of steel and had smooth surfaces.

The force and pressure distribution measurements were performed in the transonic wind tunnel [5,6] and the experiments for flow visualization were performed in the high speed wind tunnel [7,8] of the DFVLR/AVA in Goettingen.

The range of experimental work is shown in Table 1. The measurement problems result because of the requirement of covering a large Reynolds number range up to very large Reynolds number ($Re_D = 10^7$ and more) and angles of attack of up to 90° for very slender bodies with total lengths of 20 D and more. There was no wind tunnel available with a large test section within which the Mach number and Reynolds number could be varied independently within a large range. Because of this, the possibilities of experimental work was severely restricted.

3.2 Flow images and evaluation /25

The example shown in Figure 3 shows the streamlines near the wall for a body with angle of attack α = 20° from four directions over the circumference. The streamlines were made visible by means of a sprayed on mixture of oil and titanium dioxide which was sprayed on the model. The flow which reaches the body with an angle of

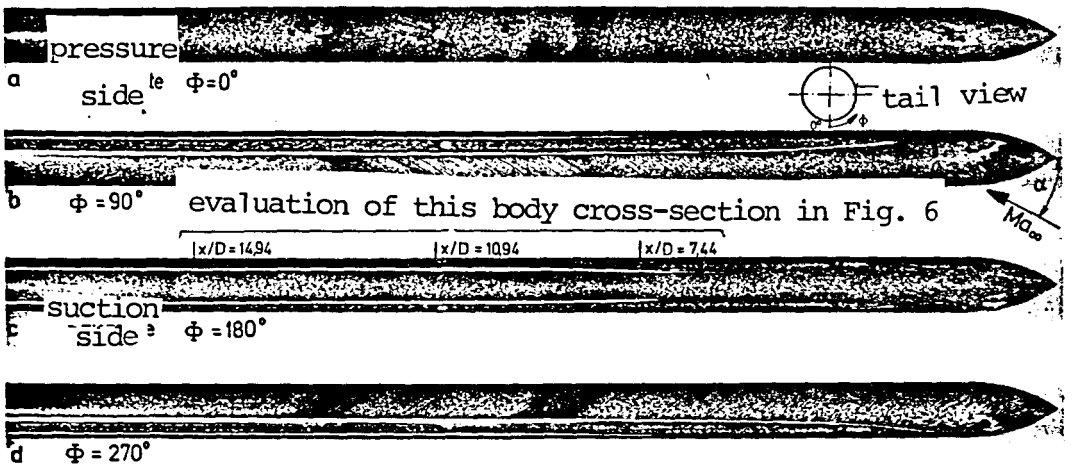

Figure 3. Paint images of body 1.
View from four directions around circumference, $\Phi = 0°$, 90°, 180° and 270°, $Ma_\infty = 0.7$ Rep $= 5.7 \cdot 10^5$, $\alpha = 20°$

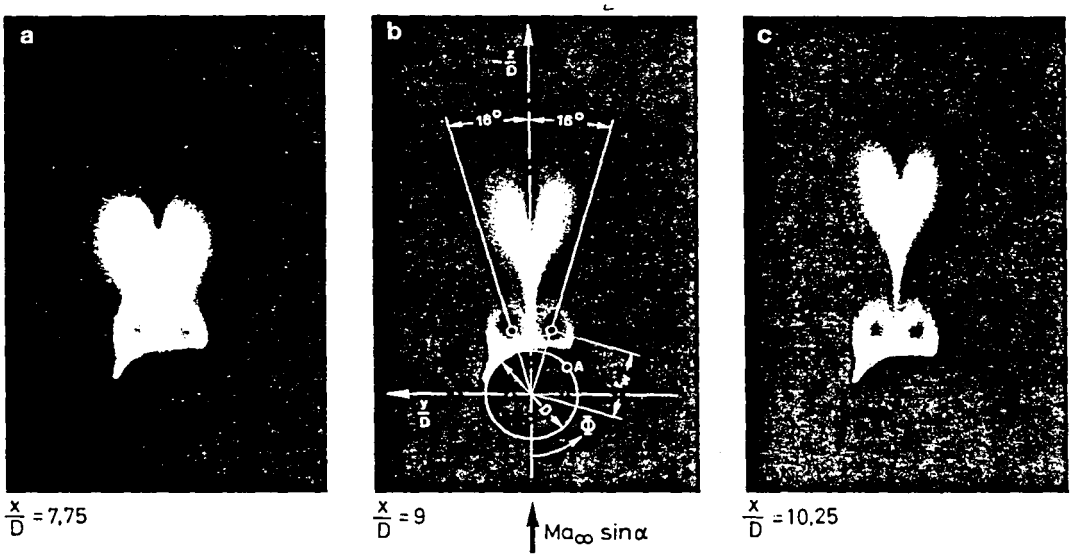

Figure 4. Smoke images of the vortex pair of body 2
$Ma_\infty = 0{,}6, Re_D = 5{,}5 \cdot 10^5, \alpha = 20°$, , light planes at $x/D = 7{,}75; 9$ and 10.25 $10{,}25; r_w/D = 0{,}75$
after probe measurements [9]

attack separates along the suction side from the body. This can be seen in Figure 3 which shows white lines running along the body. All of the streamlines coming from the pressure side merge tangentially into these separation lines. Along the separation lines, vortex layers are created which roll up over the body like cones pointing inwards, and form vortex cores which rotate in opposite directions. Such vortex cores which are made visible in perpendicular planes which respect to the body longitudinal axis using smoke are shown in Figure 4. The comparison with the vortex position found from probe measurements [9] shows good agreement with the smoke images. The smoke method can be used for high incident flow speeds as well where great difficulties occur if probe measurements are used.

Figure 3 shows two white lines along the body in the suction side quadrants which can be interpreted as primary and secondary separation lines according to the manner in which they are created. Figure 5 gives a qualitative description for this. A body cross-section has an incident flow with a transverse speed of $U_Q = U_\infty \sin\alpha$ The flow attaches at An_1, divides and flows around the body. The primary boundary layer separates again at Ab_1 and two vortex layers are produced which roll up and form the primary vortices on the suction side. The vortices form a dead water region which is limited by the backside of the body and by two streamlines which merge at the free stagnation point on the leeward side. Within the dead water region, the vortices W_1 induce down wind velocities and this makes the flow reattach at An_2. After this, the flow is directed outwards and produces a secondary boundary layer. This boundary layer separates at Ab_2, and the secondary vortices W_2 are produced. The creation of further vortices could not be found but cannot be excluded. The points Ab_1 and Ab_2 are associated with these primary and secondary separation lines mentioned above. An_3 is a separation line between them. /2

Figure 6 gives the results of a quantitative evaluation of the paint images. For three body cross-sections, and for angles of

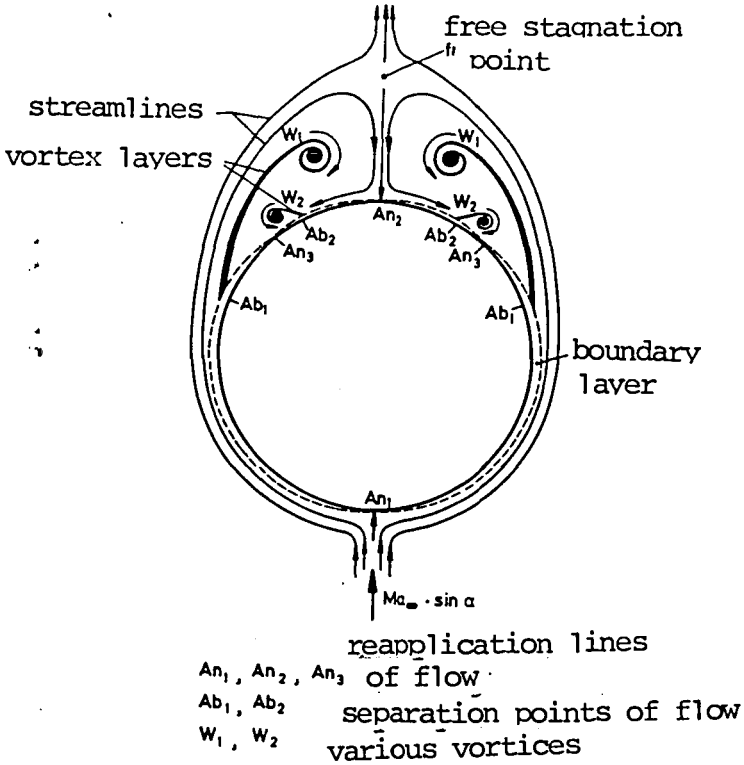

Figure 5. Schematic representation of separated body flow at the body cross-section $x/D = 10$ for $Ma_\infty = 0{,}7$, $Re_D = 5{,}7 \cdot 10^5$, $\alpha = 20°$

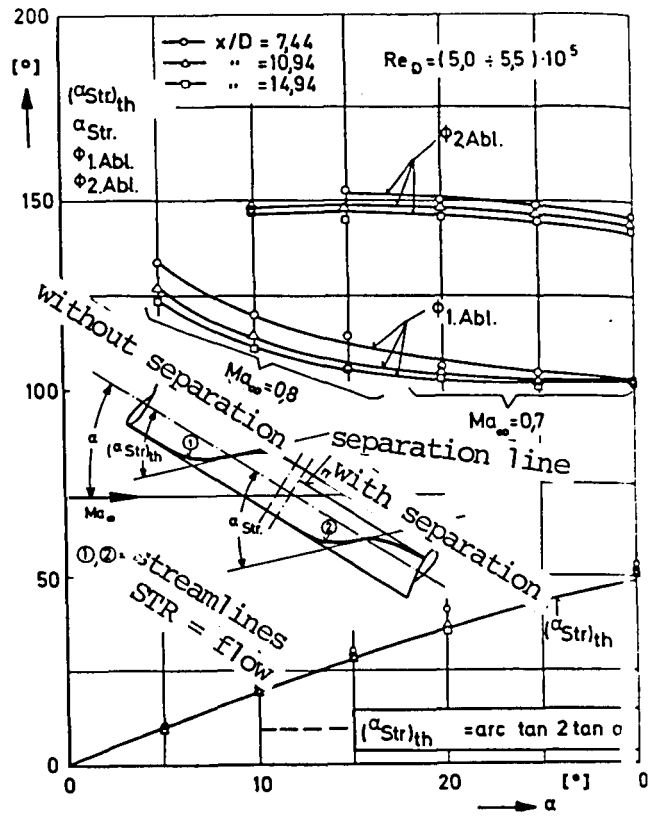

Figure 6. Separation points and streamline angles over body
Abl. = first separation, second separation

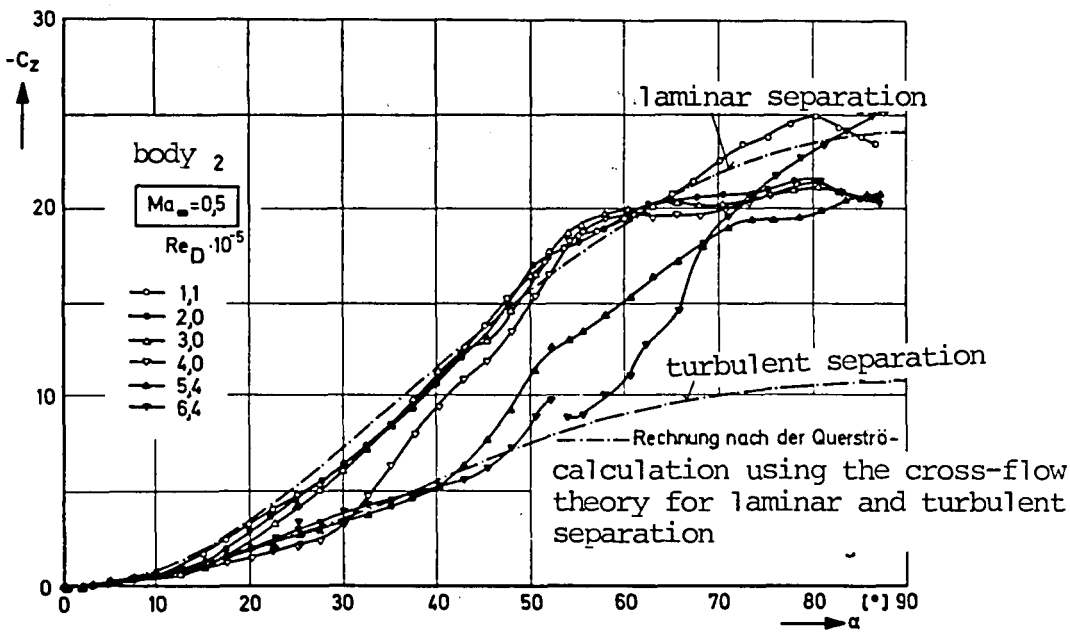

Figure 7. Normal force coefficients depending on angle of attack for variable Reynolds number of the incident flow

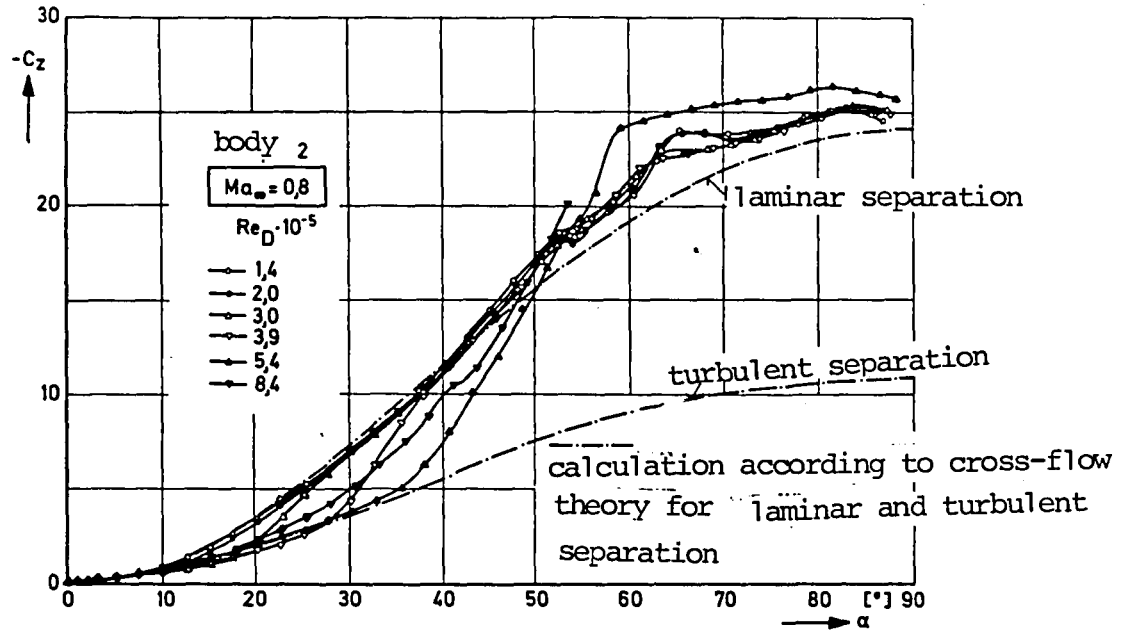

Figure 8. Normal force coefficients depending on angle of attack for variable Reynolds number of incident flow.

attack of up to $\alpha = 30°$ we show the polar angles of the primary and secondary separation, $\Phi_{1.Abl.}$ and $\Phi_{2.Abl.}$, according to the points Ab_1 and Ab_2 of Figure 5. In addition, the maximum inclination angles of the streamlines with respect to the body axis were determined. In Figure 6, this is compared with theoretical values which were calculated for incompressible potential flow. For the front part of the body cross-sections, the calculation and the experiments show slight differences, but these differences vanish almost completely for the rear cross-sections. One important parameter for the compressibility influence is the transverse flow Mach number $Ma_Q = Ma_\infty \sin\alpha$, which will be discussed later on. For the experiments, we

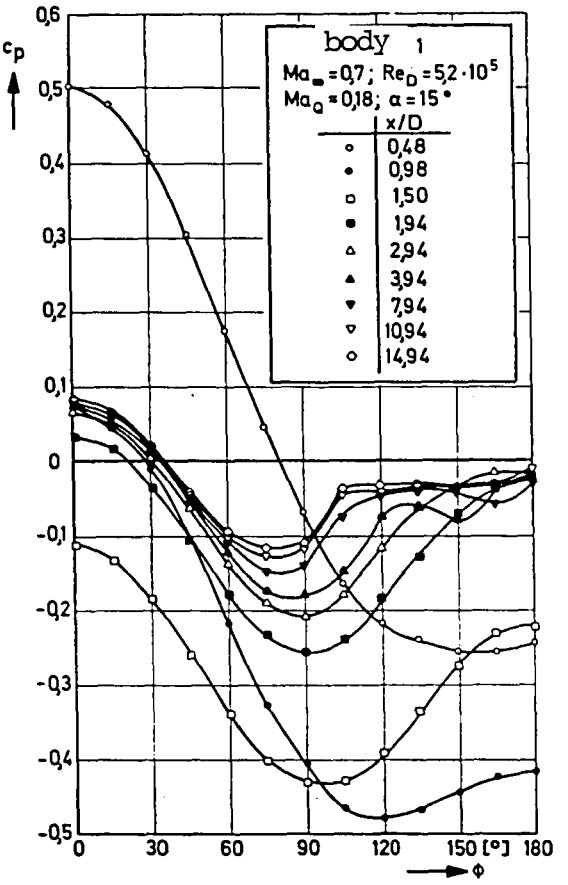

Figure 9. Pressure distributions over body surface at various body cross-sections for constant Reynolds number of incident flow.

have $Ma_Q \leqq 0{,}35$, so that a comparison with calculations still makes sense for incompressible potential flow. /2

3.3 Force measurements

A selection of the results is shown in Figures 7 and 8 which gives the normal force coefficients as a function of angle of attack for the incident Mach numbers $Ma_\infty = 0{,}5$ and 0.8 for various Reynolds numbers. The possible Reynolds number range of the transonic wind tunnel was completely exploited for the measurements. For the Mach numbers given, it extends from $Re_D = 1{,}1 \cdot 10^5$ to $8{,}4 \cdot 10^5$.

No additional devices were attached to the steel models for influencing the boundary layer transition. The large angles of attack were achieved using various offset model holders which especially in the angle of attack range between α = 55° to 90° have a somewhat disturbing influence on the measured values.

As Figures 7 and 8 show, the coefficients depend greatly on the angle of attack in a nonlinear manner. The influence of Reynolds number on the coefficients is very great and results in differences of up to 100%. Especially for small incident Mach numbers, this extends over the entire angle of attack range up to $\alpha \approx 90°$.

We will not discuss the pitch moment coefficients as a function of angle of attack here. They can be found in [1].

3.4 Pressure distribution measurements and normal force distributions

Pressure measurement distributions give important information about the details of the body flow and make it possible to determine the normal force distributions. Typical results for compressible subsonic flow can be found in Figure 9 where the pressure coefficients c_p are given as a function of polar angle Φ at α = 15°, for $Ma_\infty = 0{,}7$ and $Re_D = 5{,}2 \cdot 10^5$. This is given for various planes $x/D = \text{const}$

perpendicular to the body longitudinal axis (x = 0 at model tip). Figure 9 shows that for the flow conditions given the pressure increase on the suction side up to a cross-section occurs with a continuous increase for about twice the ogive length up to Φ = 180°. Up to here, apparently there is no flow separation. Flow separation occurs for the first time in the cross-section plane at $x/D \approx 3{,}9$ for $\Phi \approx 120°$. For body cross-sections further downstream, separation occurs at $\Phi \approx 105°$. For the circumferential angles mentioned, which correspond to the primary separation lines of Figure 3, the suction side pressure increase ends and the pressure distribution takes on a more or less constant variation. The pressure minimum in the individual cross-section distributions is displaced from large circumferential angles on the suction side of the front cross-section planes to circumferential angles of $\Phi < 90°$ for the cross-sectional areas further downstream. /28

Figures 10 and 11 give examples of the influence of Reynolds number on the pressure distributions. The transition from laminar to turbulent separation becomes apparent in Figure 10. For the Reynolds numbers $Re_D = 1{,}6 \cdot 10^5$ and $2.4 \cdot 10^5$, separation occurs already for the circumferential angle $\Phi \approx 60°$, , which indicates laminar separation. For all other cases, separation apparently is turbulent at $\Phi \approx 120°$.

For small transverse slow Mach numbers, the separation is controlled by Reynolds number. With increasing transverse flow Mach number, the Reynolds number influence is almost reduced to zero, as can be seen in Figure 11. For the over critical transverse flow Mach numbers, separation occurs similar to laminar separation for circumferential angles of between Φ = 60° to 80°. Further details, especially an explanation of the critical transverse flow Mach number and circular cylinder flow, are contained in [1].

Using numerical integration of the measured pressure distributions, the local normal force coefficients are calculated. These

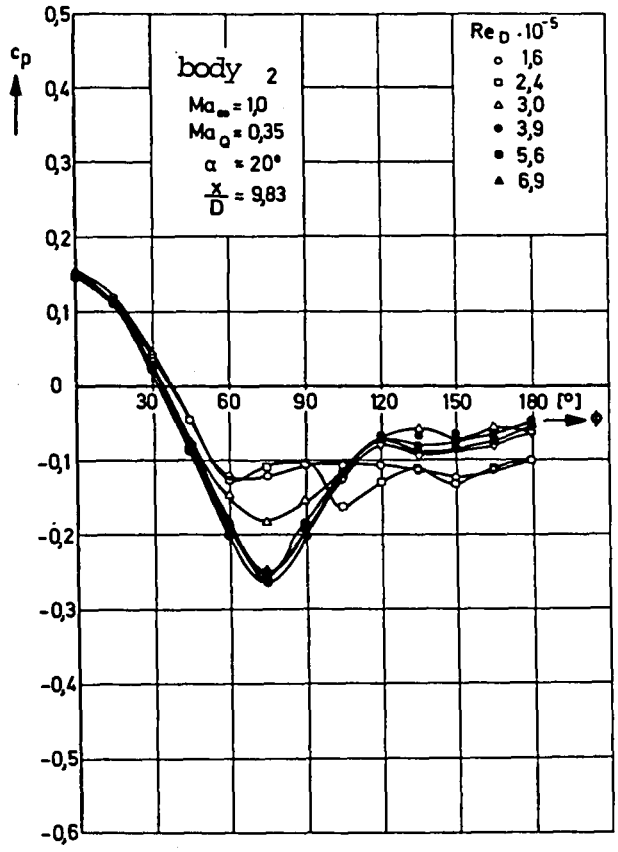

Figure 10. Pressure distributions along body surface for variable Reynolds number of incident flow.

extensive results are shown by Figures 12 to 14 which gives the normal force distribution.

Along the ogive the local normal forces increase greatly and depending on Mach number, after one-half to two-thirds of the ogive length, they can reach maximum values and then decrease rapidly. Various transition regions occur behind which the local normal force coefficients are given by constant values or this may be a good approximation. The normal force distributions in Figure 12 results from pressure distributions as shown in Figure 8. These are based on turbulent separation.

As already mentioned, for over critical transverse flow Mach numbers, the flow separates from the body just like for laminar

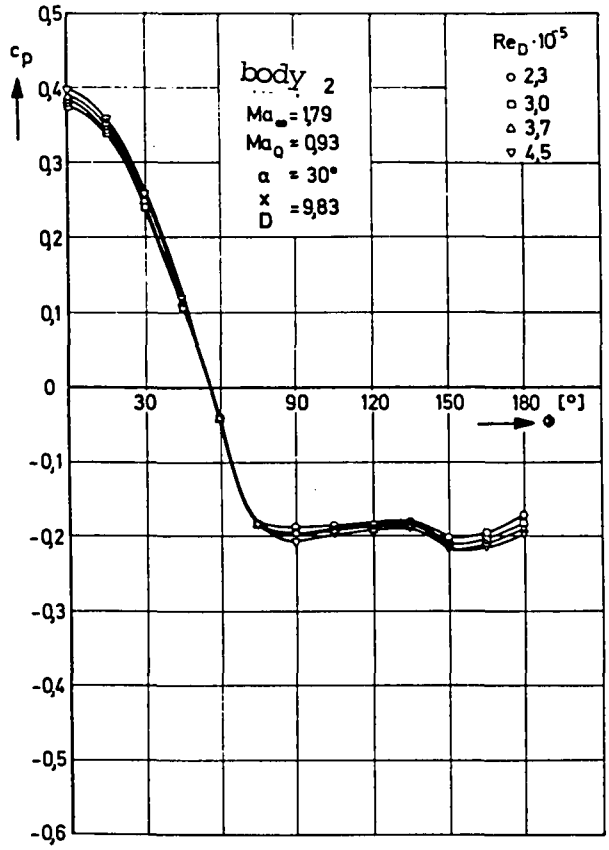

Figure 11. Pressure distributions over body surface for variable Reynolds number of incident flow.

separation. Because of the large dead water region with reduced pressures, large local normal forces occur along the body as shown in Figure 13. These normal force distributions can be attributed to the pressure distributions given in Figure 10 for angles of attack of $\alpha > 13°$.

/3

Figure 14 gives examples of normal force distribution for variable Reynolds number which are given here without comment. They are intended to give the reader a complete overview of the experimental work.

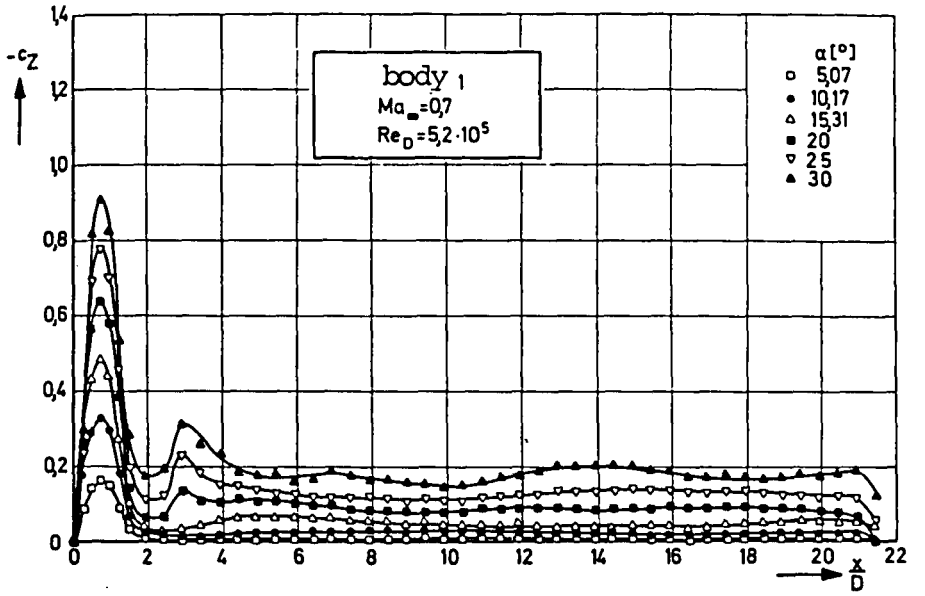

Figure 12. Normal force distributions for constant Reynolds number of incident flow.

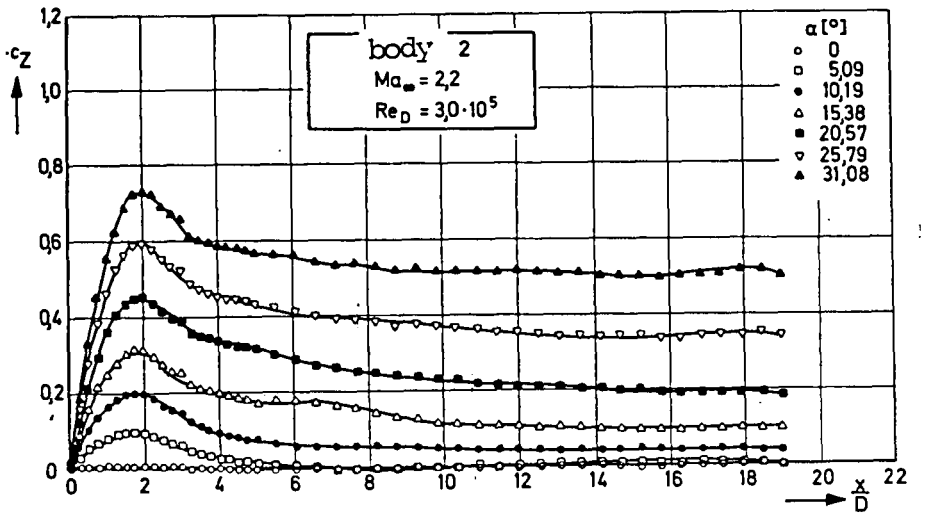

Figure 13. Normal force distributions for constant Reynolds number of incident flow.

4. Theoretical analysis of the experimental results

4.1 Theoretical calculation methods and comparison with measurements

An exact treatment of the flow field around bodies with high angles of attack is not possible today. The approximate methods known from the literature are of the empirical or semi-empirical type and can be summarized with the term "transverse flow theory". H. J. Allan and E. W. Perkins [10,11] make the assumption that the total normal force on the body consists of a frictionless part (potential transverse force) and a friction part (friction transverse force). In order to determine the potential transverse force, Allan and Perkins use a simple method of M. M. Munk [12] which is based on the momentum theorum. It applies for relatively slender bodies in frictionless incompressible flow and, therefore, is restricted to very small angles of attack. This method was developed in the analysis of balloon bodies. Methods for determining the friction lift for such closed bodies of revolution were given by H. Multhopp [13] and X. Hafer [14]. Projectile bodies differ from these body shapes because of a large ratio of length to diameter, the fact that the cross-section is for the most part constant, and because the tail is blunt. For such bodies, Allan and Perkins determined the friction transverse force by associating a circular cylinder with the transverse flow speed $U_Q = U_\infty \sin\alpha$ to each body cross section, and a difference is made between laminar and turbulent separation.

H. R. Kelly [15] further developed the method of Allan and Perkins. Based on an analogy between the stationary, three-dimensional flow around a projectile body and the unsteady two-dimensional flow of a circular cylinder which is suddenly set in motion from rest, the nonlinear, local normal force is set equal to the instantaneous drag (per unit of length) of a circular cylinder having the transverse flow speed U_Q. The time coordinate of the unsteady case is associated with the space longitudinal coordinate of the body.

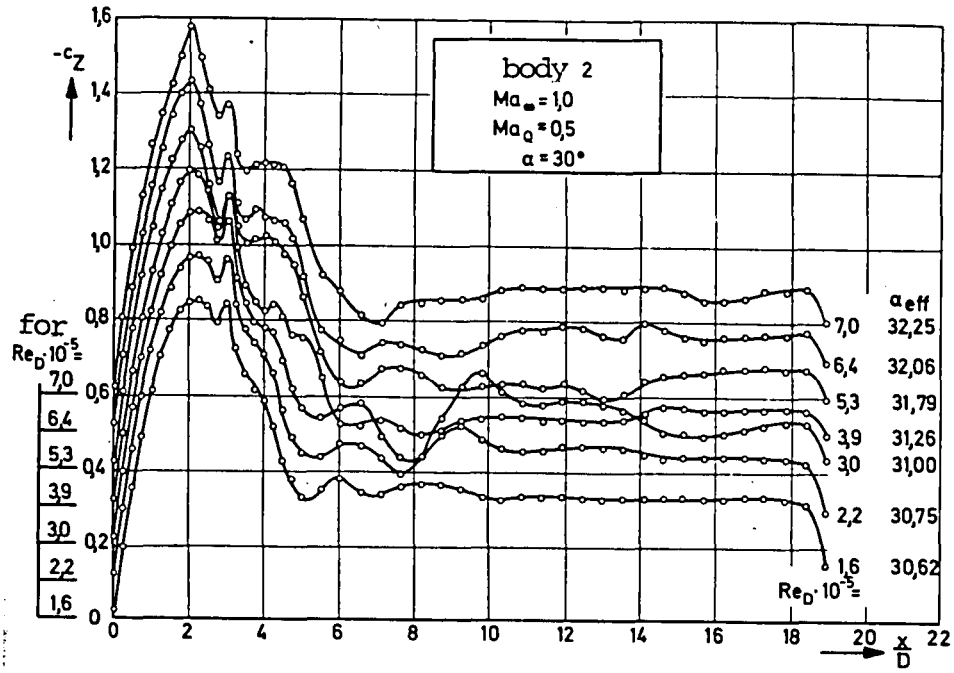

Figure 14. Normal force distribution for constant Reynolds number of incident flow.

The method of Kelly was expanded greatly by K. D. Thomson [16], especially by introducing a number of empirical corrections for various influences, for example, pressure gradients at the model head, various tail geometries, etc.

Both Kelly and Thomson use the assumption of Allan and Perkins that the total normal force is the sum of the potential transverse force and the friction transverse force. The unsteady drag coefficients for determining the distribution of the friction transverse force were taken from test results which were obtained first by M. Schwabe [17] and later on in improved form by T. Sarpkaya [18]. The results of these experimental investigations for circular cylinders suddenly accelerated to a constant final speed are represented by the drag function shown in Figure 15. This drag function applies for laminar separation from the cylinder. For the more important practical case of turbulent separation, no experimental data is available. Kelly uses, therefore, a function for turbulent separation which is obtained from the one for laminar separation multiplied

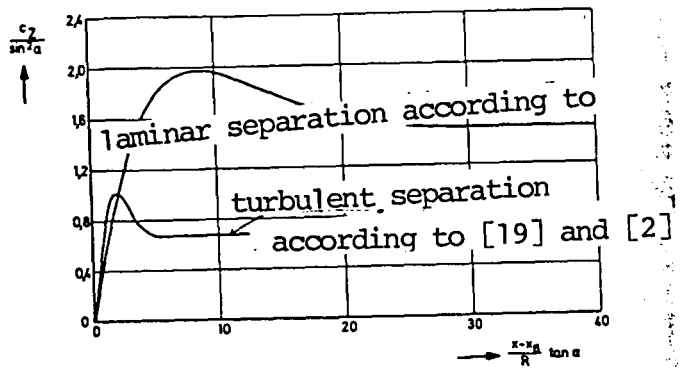

Figure 15. Local normal force coefficients over body of projectile for laminar and turbulent separation.

by a factor which equals the ratio of the stationary turbulent drag coefficient and the stationary laminar drag coefficient. Thomson gives this factor as a function of angle of attack.

One can object to the method discussed above because the boundary layers of the body with angle of attack and the boundary layer of the circular cylinder, in general, are not the same. Consequently, the separation process leads to different values for the local normal force and the unsteady and stationary drag. In the best case, the equality of local normal force and drag for laminar boundary layer could be expected because only for this case is the transverse component of speed independent of the longitudinal component. For this reason and because no experimental data was available for unsteady drag coefficients force turbulent separation, E. Wedemeyer [19] determined the corresponding function from extensive measurements of K. Hartmann [2] and the result given by Schwabe and Sarpkaya. Figure 15 also gives this function determined using the unsteady analogy discussed above, in addition to the drag function of Sarpkaya. Comparison shows that the turbulent coefficients differ not only by a constant factor from the laminar one but also the turbulent coefficients is more condensed in the direction of the abscissa. This means that in the case of turbulent separation for the unsteady problem, the stationary end value is reached much earlier.

Recent work by F. J. Marshall and F. D. Deffenbaugh [20] and F. D. Deffenbaugh and W. G. Koerner [21] also using the unsteady transverse flow analogy, attempt to use no empirical input data at all. The application range of these methods is also limited and the results obtained with them can only be made to agree with experimental results using an empirical factor which depends on body geometry. /3

According to the transverse flow theory, we find the following calculation of the coefficient of normal force

(1)

$$-C_Z = \sin 2\alpha + \frac{4\sin^2\alpha}{\pi} \int_{x_B/D}^{L_R/D} C_W \, d\left(\frac{x}{D}\right).$$

The first term on the right side of equation (1) is the part of the potential transverse force. It is obtained from the theory of slender bodies for incompressible potential flow. The second term of equation (1) is the part of the friction transverse force. It was calculated using the drag function shown in Figure 15, and because of the different reference quantities of the normal force coefficients and the drag coefficients, the ordinant values still had to be multiplied with $\pi/4$. The further analysis is the nonlinear normal force part caused by friction. The results of the calculations for the normal force are shown in Figures 7 and 8 for comparison with measurements. As the comparison shows, the measurements first follow the calculation for turbulent separation for all Reynolds numbers, go slightly below this curve and then transfer to the curve calculated for laminar separation with a clear increase. This transition occurs for ever larger angles of attack with increasing Reynolds number. In the next section we will give an explanation for this behavior.

4.2 Representation of the nonlinear normal force part as a function of the effective Reynolds number

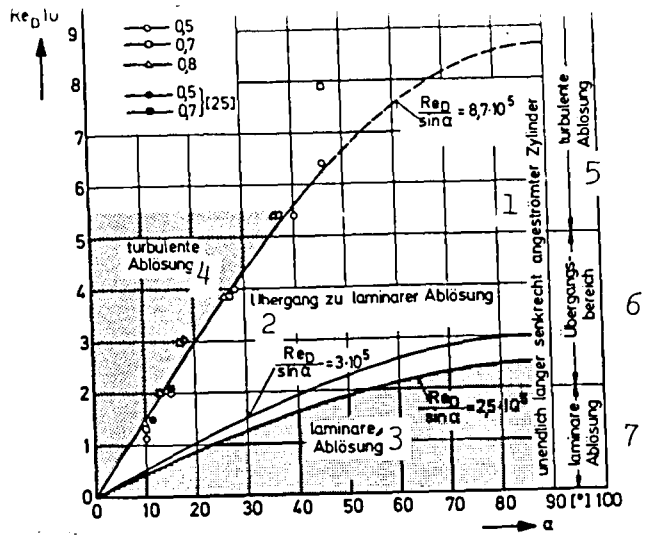

1--Infinitely long cylinder perpendicular to flow 2--transition to laminar separation
3--laminar separation 4--turbulent separation 5--turbulent separation
6--transition range 7--laminar separation

Figure 16. Limiting curves for laminar and turbulent separation over body.

One obtains an important result by showing the correspondence of those Reynolds numbers and those angles of attack, at which the measurements of the curve calculated for turbulent separation transfer to the calculated curve for laminar separation with a large increase given in Figures 7 and 8. Figure 16 shows the transition points by dots obtained from measurements. They should not be considered measurement points. They can be represented by a single curve and the following relationship results.

(2) $$\frac{Re_D}{\sin\alpha} = 8{,}7\cdot10^5 \,(= Re_{eff}), \quad \text{valid for } \alpha > 5°.$$

Equation (2) defines an effective Reynolds number for the following analysis. Using this empirically found function, we have a limiting curve which encloses the Reynolds number--angle of attack pairs together with the ordinate within which the flow separates in a turbulent manner. To the right side of it, we have the region of transition to laminar separation. This region has to be limited by an additional curve for Reynolds numbers $Re_D < 2\cdot10^5$ and on its right side, only laminar separation occurs. It cannot be directly determined from the present measurements due to the reasons mentioned in [1] and, therefore, it was determined indirectly from the universal empirical function in Figure 19 still to be described.

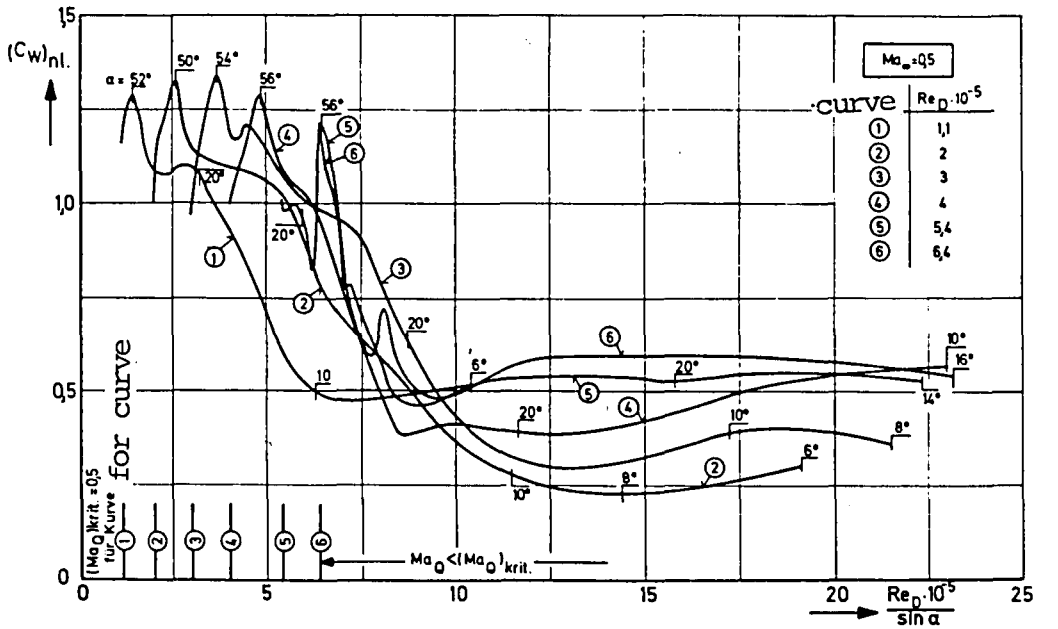

Figure 17. Nonlinear normal force coefficients represented as drag coefficients dependent on the effective Reynolds number.

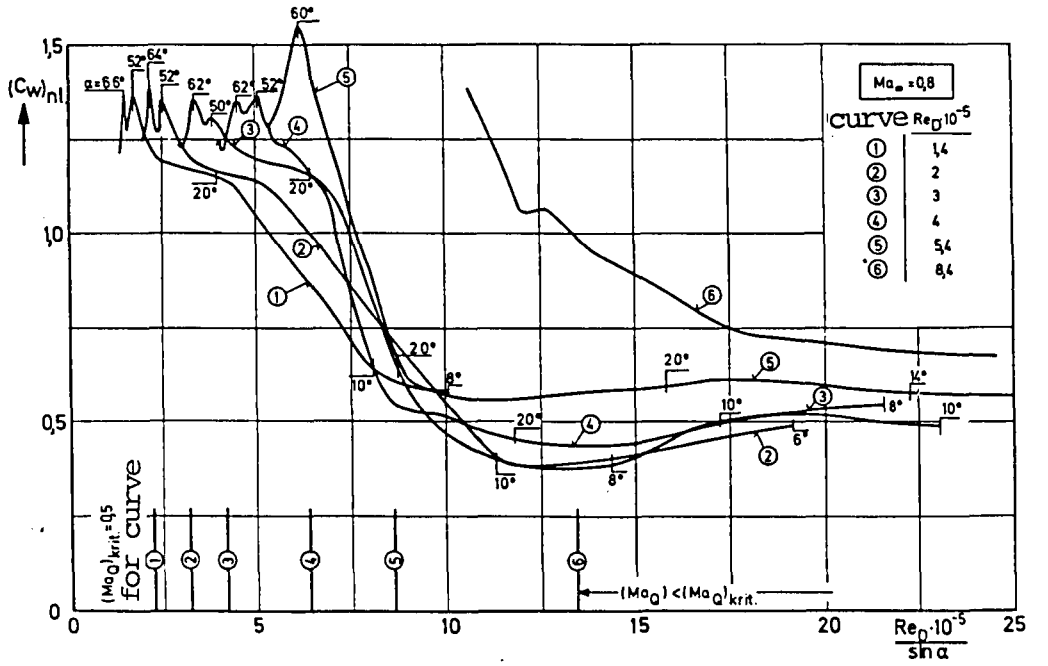

Figure 18. Nonlinear normal force coefficients represented as drag coefficients depending on an effective Reynolds number.

Using the effective Reynolds number $Re_D/\sin\alpha$ defined here, it is possible to classify separation over a body with angle of attack in a physically more correct manner than if one uses the transverse flow Reynolds number $Re_D \sin\alpha$. used by many authors. The latter is usually not a criterion for whether or not separation is laminar or turbulent. For smaller angles of attack, the transverse flow Reynolds number is very small and, therefore, one would expect laminar separation. In contrast to this, for small angles of attack the running lengths of the streamlines over the body are very large and turbulent separation occurs. The lengths characteristic for the true conditions is the running length of the streamlines. The author has already indicated this in [4] and it is also mentioned in H. Esch [22]. The length of the streamlines near the wall up to the separation points is a function of the angle of attack and is approximately defined by the effective Reynolds number by means of $D/\sin\alpha = f(\alpha)$. Therefore, if one goes through an angle of attack range, the effective Reynolds number is also simultaneously changed. Therefore, angles of attack smaller than 5° are excluded for the range of validity of the effective Reynolds number. In this range, linear, potential theory methods give sufficiently accurate results.

We now have to deal with the question of the dependence of the nonlinear normal forces on the effective Reynolds number defined here. According to the transverse flow theory, the nonlinear normal force parts is associated with the drag of the circular cylinder. This means that at least in the incompressible subsonic range, a similar Reynolds number dependent like for the circular cylinder would be expected. In order to establish the presumed relationship, the nonlinear normal force parts from force measurements were split off and were plotted in the form of an analog drag coefficient as a function of effective Reynolds number shown in Figures 17 and 18. The nonlinear normal force parts were calculated from the measured total forces according to the following equation

(3) $$(C_Z)_{nl.} = C_Z - \sin 2\alpha.$$ /32

The term sin 2α results, as already mentioned, from the theory of slender bodies for incompressible potential flow. The recalculation of the nonlinear normal force coefficient to the reference quantities of the circular cylinder leads to the following:

$$(C_W)_{nl.} = \frac{(C_Z)_{nl.}}{\sin^2\alpha} \frac{\pi}{4} \frac{D}{L_Z}. \tag{4}$$

The drag coefficients calculated according to equation (4) are given in Figures 17 and 18. All of the curves have a qualitative behavior which corresponds to the transfer from undercritical to overcritical Reynolds numbers in the case of a circular cylinder. For the values of the body, the critical region starts approximately for the effective Reynolds number of $Re_D/\sin\alpha = 5 \cdot 10^5$, and the corresponding Reynolds number of the circular cylinder is $Re_D = 2 \cdot 10^5$. With increasing incident Mach number and, therefore, transverse flow Mach number, the $(C_W)_{nl.}$ values over the entire investigated range increase somewhat. For constant effective Reynolds number, a different transverse flow Mach number corresponds to each curve of Figures 17 and 18. Along each individual curve the transverse flow Mach number is not constant. It increases from the right to the left when passing through the curves, depending on angle of attack. For orientation, the curves have various marked angles of attack. The transverse flow Mach number takes on these values which extends from incompressible flow up to critical and even overcritical incident flow. In Figures 17 and 18, along the abscissa, we show the effective Reynolds number at which the individual curves reach the critical transverse flow Mach number. The critical transverse flow Mach number was assumed to be $(Ma_Q)_{krit.} = 0{,}5$, that is somewhat larger than the potential--theory critical value of the circular cylinder. On the right side of these marks, the transverse flow Mach number is smaller than the critical one and it is larger on the left side.

With the exception of the case given in curve 6 of Figure 18, in all of the other cases the transition from turbulent to laminar separation occurs before reaching the critical transverse flow Mach number. For curve 6, the relatively sudden drag increases apparently

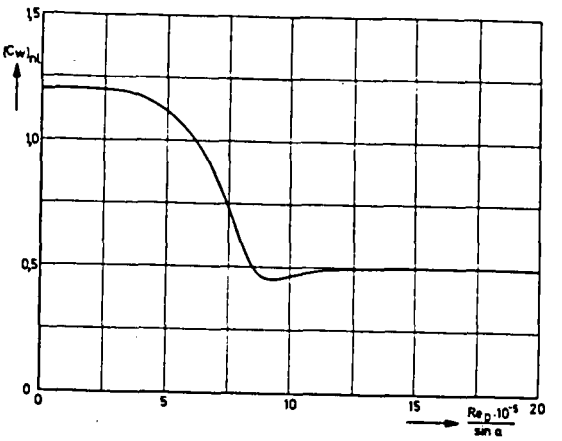

Figure 19. Universal empirical function for the non-linear normal force and pitch moment coefficient in the form of a drag coefficient depending on an effective Reynolds number.

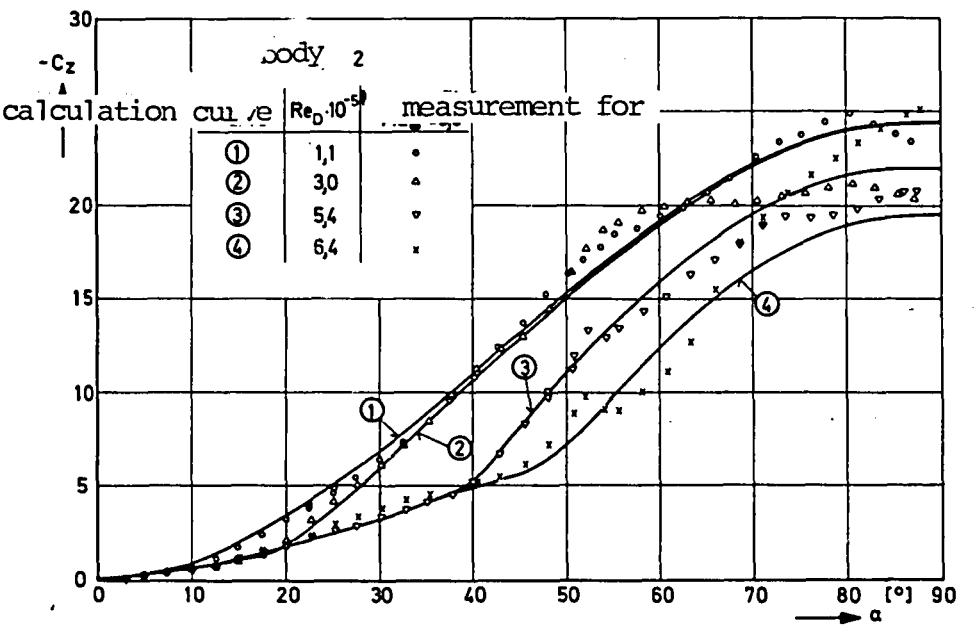

Figure 20. Normal force coefficient depending on angle of attack for various Reynolds numbers, comparison of calculation and measurements.

caused by reaching the critical transverse flow Mach number. The transverse flow Mach number and the effective Reynolds number are coupled and experimentally, it is not possible to vary the effective Reynolds number over a wide range for different transverse flow Mach numbers when they are held constant in order to determine their effects separately.

4.3 Calculation of normal forces using a universal empirical function

The curves in Figures 17 and 18 can be roughly approximated by a single curve. This can be used as a universal empirical function for describing an analog drag coefficient for projectile bodies as a function of the effective Reynolds number. In Figure 19, we show the variation of the universal empirical function from the results of the previous chapter. Since there is a certain subjective influence inside the limits defined by curves 1 to 5 of Figures 17 and 18, for orientation, the drag variation of a circular cylinder was used [23,24,25]. Various details of the deviations of the experimental values from the basic trends given by the universal empirical function are discussed in detail in [1].

Starting with the drag function given in Figure 19, the normal forces of the body were calculated for several examples in order to test the usability of this function. As examples, we mention here the calculated normal force coefficients for $Ma_\infty = 0{,}5$ and 0.8 for various Reynolds numbers. They are given in Figures 20 and 21 together with the corresponding measurement values. The comparison of measurement and calculation shows that using the empirically found universal drag function, one can satisfactorily represent the effects which depend on Reynolds number.

The influence of Mach number is not contained in the universal drag function. This means that if one exceeds the critical transverse flow Mach number, the calculation gives normal force coefficients

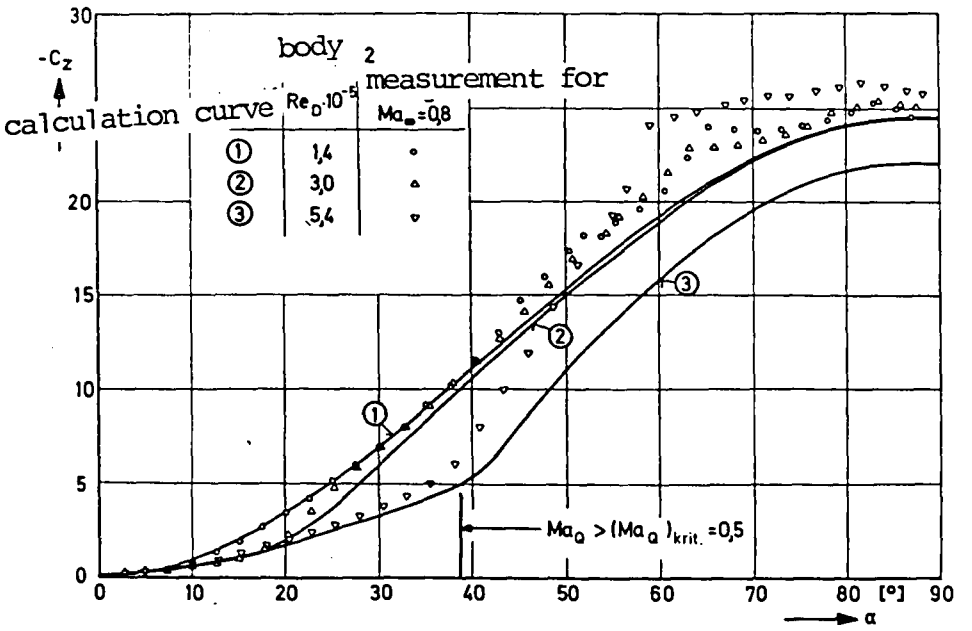

Figure 21. Normal force coefficients depending on angle of attack for different Reynolds numbers, comparison of calculation and measurement.

which are too small as shown in Figure 21. Strictly speaking, the universal drag function should be limited to the range of incompressible transverse flow Mach numbers. The calculated values, however, show that satisfactory results are obtained in this way for the entire range of undercritical transverse flow. The influence of Mach number could be considered by an additional empirical correction.

5. Summary

New extensive experimental work of projectile body models with angles of attack of up to 90° was reported on. The experiments include force and moment measurements, pressure distribution measurements and flow visualizations using paint images and smoke photographs of body vortices. In the investigations, the influence of Reynolds number on the aerodynamic forces was of primary importance. A theoretical analysis of the experimental results led to the definition of an effective Reynolds number and to the representation of its influence on the aerodynamic coefficients. This effective Reynolds number considers the pathlengths of the streamlines with its

characteristic length and has been found to be a usable criterion for evaluating whether or not separation over the body is laminar or turbulent. The nonlinear normal force parts can be represented by only one function in the form of an analog drag coefficient of the circular cylinder as a function of effective Reynolds number. The normal forces and pitch moments calculated according to the transverse flow theory using this function give satisfactory results over the entire range of undercritical transverse flow Mach numbers.

REFERENCES

[1] K. Hartmann: Influence of Reynolds number on the normal forces of slender projectile bodies. Dissertation TU Braunschweig 1976, extended version. Internal DFVLR AVA-Report 25176A20 (1976).

[2] K. Martmann: Aerodynamic investigations of projectiles in the transonic speed range. Part II. Systematic pressure distribution measurements. Internal AVA Report 69A06 (1969).

[3] W. Stahl, K. Hartmann, W. Schneider: Suggestions for research work on projectiles with small aspect ratio wings at the AVA, in collaboration with the Royal Aircraft Establishment, Farnborough, England. AVA Memorandum (1969).

[4] K. Hartmann: Three component measurements and pressure distribution measurements including flow observations of a circular cylinder projectile body with various head shapes at Mach numbers of Ma_∞ = 0.5 to 2.2 and various Reynolds numbers internal DFVLR/ AVA report 25174A32 (1974).

[5] H. Ludwieg, W. Lorenz-Meyer, W. Schneider: The transonic wind tunnel of the aerodynamic test facility Goettingen year book 1966 of the WGLR pg. 145-155.

[6] Th. Hottner and W. Lorenz-Meyer. The transonic wind tunnel of the aerodynamic test facility Goettingen (second development stage) yearbook 1968 of the DGLR, pg. 233-244.

[7] H. Ludwieg and Th. Hottner: The high speed wind tunnel of the aerodynamic test facility Goettingen. Z. Flugwiss. 7 (1959), pg. 294-299.

[8] H. Ludwieg and Th. Hottner: The supersonic test section (710 mm x 725 mm) of the high speed wind tunnel of the AVA. Z. Flugwiss. 11. 11 (1963), pg. 137-142.

[9] F. R. Grosche: Wind tunnel investigations of the vortex system of a body revolution with angle of attack with and without wing. Z. Flugwiss. 18 (1970, p. 208-217.

[10] H. J. Allen and E. W. Perkins: A study of effects of viscosity on flow over slender inclined bodies of revolution. NACA Rep- 1048 (1951).

[11] H. J. Allen: Estimation of the forces and moments acting on inclined bodies of revolution of high fineness ratio. NACA RM A9126 (1949).

[12] M. M.Munk: The aerodynamic forces on airship hulls. NACA Rep. 184 (1924). Siehe auch M. M. Munk: Aerodynamics of airships. In: W. F. Durand (Herausgeber): Aerodynamic Theory, Vol. VI. Julius Springer, Berlin 1936. Reprint Dover Publications, New York 1963.

[13] H. Multhopp: The aerodynamics of an aircraft body. Luftfahrtforsch. 18 (1941), p. 52-66.

[14] X. Hafer: Investigations of the aerodynamics of wing body configurations. Dissertation TH Braunschweig 1957. Yearbook 1957 of the WGL, p. 191-207.

[15] H. R. Kelly: The estimation of normal force, drag and pitching moment coefficients for blunt based bodies of revolution at large angles of attack. J. Aeron. Sci. 21 (1954), p. 549-56.

[16] K. D. Thomson: The estimation of viscous normal force, pitching moment, side force and yawing moment on bodies of revolution at incidences up to 90°. WRE-Report 782, Salisbury, South Australia (1972).

[17] M. Schwabe: Determining pressure in the nonsteady plane flow. Ing-Arch. 6 (1935), p. 34-50. English translation: Pressure distribution in nonuniform two-dimensional flow. NACA TM 1039 (1943).

[18] T. Sarpkaya: Separated flow about lifting bodies and impulsive flow about cylinder. AIAA Journ. 4 (1965), p. 414-420.

[19] E. Wedemeyer: Lift distribution of slender wing-body combination with separated flow. Internal DFVLR/AVA report 25173A32 (1974).

[20] F. J. Marshall and F. D. Deffenbaugh: Separated flow over a body of revolution, J. Aircraft 12 (1975), p. 78-85.

[21] F. D. Deffenbaugh and W. G. Koerner: Asymmetric vortex wake development on missiles at high angles of attack. J. Spacecraft 14 (1977), p. 155-162.

[22] H. Esch: Influence of Reynolds number on normal force characteristics of slender cylindrical bodies. Deutsche Luft- und Raumfahrt, FB 75-09 (1975).

[23] F. E. Gowen and E. W. Perkins: Drag of circular cylinders for a wide range of Reynolds numbers and Mach numbers. NACA TN 2960 (1952).

[24] A. Roshko: Experiments on the flow past a circular cylinder at very high Reynolds number. J. Fluid Mech. 10 (1960, p. 345-56.

[25] P. Bublitz. Experimental investigations of flow over a circular cylinder performing harmonic oscillations in a transverse flow. Interval DFVLR/AVA report 71J22 (1971).

End of Document